Simultaneous Measurement of Proton and Lepton Kinematics in Quasielasticlike ν_μ-Hydrocarbon Interactions from 2 to 20 GeV

D. Ruterbories,[1] S. Akhter,[2] Z. Ahmad Dar,[3,2] F. Akbar,[2] V. Ansari,[2] M. V. Ascencio,[4,*] M. Sajjad Athar,[2] A. Bashyal,[5,†] A. Bercellie,[1] M. Betancourt,[6] A. Bodek,[1] J. L. Bonilla,[7] A. Bravar,[8] H. Budd,[1] G. Caceres,[9,‡] T. Cai,[1] M. F. Carneiro,[5,9,§] G. A. Díaz,[1] H. da Motta,[9] J. Felix,[7] L. Fields,[10] A. Filkins,[3] R. Fine,[1,∥] A. M. Gago,[4] H. Gallagher,[11] P. K. Gaur,[2] A. Ghosh,[12,9] S. M. Gilligan,[5] R. Gran,[13] E. Haase,[13] D. A. Harris,[14,6] S. Henry,[1] K. Jacobsen,[13] D. Jena,[6] S. Jena,[15] J. Kleykamp,[1,¶] A. Klustová,[16] M. Kordosky,[3] D. Last,[17] A. Lozano,[9] X.-G. Lu,[18,19] E. Maher,[20] S. Manly,[1] W. A. Mann,[11] C. Mauger,[17] K. S. McFarland,[1] A. M. McGowan,[1] B. Messerly,[21,**] J. Miller,[12] O. Moreno,[3,7] J. G. Morfín,[6] D. Naples,[21] J. K. Nelson,[3] C. Nguyen,[22] A. Olivier,[1] V. Paolone,[21] G. N. Perdue,[6,1] K.-J. Plows,[19] M. A. Ramírez,[17,7] R. D. Ransome,[23] H. Ray,[22] H. Schellman,[5] C. J. Solano Salinas,[24] H. Su,[21] M. Sultana,[1] V. S. Syrotenko,[11] E. Valencia,[3,7] N. H. Vaughan,[5] A. V. Waldron,[16] M. O. Wascko,[16] C. Wret,[1] B. Yaeggy,[12,††] and L. Zazueta[3]

(MINERvA Collaboration)

[1]*Department of Physics and Astronomy, University of Rochester, Rochester, New York 14627, USA*
[2]*AMU Campus, Aligarh, Uttar Pradesh 202001, India*
[3]*Department of Physics, William and Mary, Williamsburg, Virginia 23187, USA*
[4]*Sección Física, Departamento de Ciencias, Pontificia Universidad Católica del Perú, Apartado 1761 Lima, Perú*
[5]*Department of Physics, Oregon State University, Corvallis, Oregon 97331, USA*
[6]*Fermi National Accelerator Laboratory, Batavia, Illinois 60510, USA*
[7]*Campus León y Campus Guanajuato, Universidad de Guanajuato, Lascurain de Retana No. 5, Colonia Centro, Guanajuato 36000, Guanajuato, México*
[8]*University of Geneva, 1211 Geneva 4, Switzerland*
[9]*Centro Brasileiro de Pesquisas Físicas, Rua Dr. Xavier Sigaud 150, Urca, Rio de Janeiro, Rio de Janeiro 22290-180, Brazil*
[10]*Department of Physics, University of Notre Dame, Notre Dame, Indiana 46556, USA*
[11]*Physics Department, Tufts University, Medford, Massachusetts 02155, USA*
[12]*Departamento de Física, Universidad Técnica Federico Santa María, Avenida España 1680 Casilla 110-V, Valparaíso, Chile*
[13]*Department of Physics, University of Minnesota—Duluth, Duluth, Minnesota 55812, USA*
[14]*York University, Department of Physics and Astronomy, Toronto, Ontario M3J 1P3, Canada*
[15]*Department of Physical Sciences, IISER Mohali, Knowledge City, SAS Nagar, Mohali—140306 Punjab, India*
[16]*The Blackett Laboratory, Imperial College London, London SW7 2BW, United Kingdom*
[17]*Department of Physics and Astronomy, University of Pennsylvania, Philadelphia, Pennsylvania 19104, USA*
[18]*Department of Physics, University of Warwick, Coventry CV4 7AL, United Kingdom*
[19]*Oxford University, Department of Physics, Oxford OX1 3PJ, United Kingdom*
[20]*Massachusetts College of Liberal Arts, 375 Church Street, North Adams, Massachusetts 01247, USA*
[21]*Department of Physics and Astronomy, University of Pittsburgh, Pittsburgh, Pennsylvania 15260, USA*
[22]*University of Florida, Department of Physics, Gainesville, Florida 32611, USA*
[23]*Rutgers, The State University of New Jersey, Piscataway, New Jersey 08854, USA*
[24]*Facultad de Ciencias, Universidad Nacional de Ingeniería, Apartado 31139, Lima, Perú*

(Received 23 March 2022; revised 25 May 2022; accepted 21 June 2022; published 6 July 2022)

Neutrino charged-current quasielastic-like scattering, a reaction category extensively used in neutrino oscillation measurements, probes nuclear effects that govern neutrino-nucleus interactions. This Letter reports the first measurement of the triple-differential cross section for ν_μ quasielastic-like reactions using the hydrocarbon medium of the MINERvA detector exposed to a wideband beam spanning $2 \leq E_\nu \leq 20$ GeV. The measurement maps the correlations among transverse and longitudinal muon momenta and summed proton kinetic energies, and compares them to predictions from a state-of-art simulation. Discrepancies are observed that likely reflect shortfalls with modeling of pion and nucleon intranuclear scattering and/or spectator nucleon ejection from struck nuclei. The separate determination of leptonic and hadronic variables can inform experimental approaches to neutrino-energy estimation.

DOI: 10.1103/PhysRevLett.129.021803

Current and future long baseline neutrino experiments [1–4] seek to delineate the neutrino mass ordering and to quantify the presence of charge-parity violation in the neutrino sector. These experiments will use neutrinos of energies from 0.3 to 4 GeV and higher if tau-neutrino appearance is explored [5]. Accurate models of neutrino-nucleus interactions are required to relate the energies of visible final-state particles of events observed in the detectors to the initiating true neutrino energies that underwrite the oscillations of neutrino flavor. A leading contributor to charged-current neutrino interactions at these energies is the quasielastic-like channel:

$$\nu_\mu + \mathcal{A} \to \mu^- + \text{nucleons} + A'. \tag{1}$$

Charged-current neutrino interactions within nuclei, even those with apparent two-body quasielastic final states, are altered by a number of poorly understood effects: The struck nucleons of the initial state are bound and in motion [6,7]; short-range multinucleon processes give rise to enhanced reaction rates relative to scattering on free nucleons [8–13], and hadrons produced in the parent ν_μ interactions with nucleons undergo intranuclear final-state interactions (FSI) within the target nuclei. While the reaction $\nu_\mu + \mathcal{A} \to \mu^- + p + \mathcal{A}'$, wherein nearly all final-state energy is visible, is thought to be the main contributor to the quasielastic-like channel [Eq. (1)] a significant number of events may have energy deposited in undetected neutrons or light nuclear fragments. Final states of the latter kind complicate the task of inferring neutrino energy from samples of quasielastic-like events.

The reaction of Eq. (1) has received repeated experimental scrutiny; however only single- or double-differential cross sections in muon kinematics have been reported, mostly carried out with ν_μ of incident energies, E_ν, of sub-GeV to few GeV [14–31]. This Letter reports a new measurement of the quasielastic-like channel in which the final-state muon transverse (p_t) and longitudinal ($p_{\|}$) momenta are measured in each event simultaneously with the total "available" (calorimetrically visible) recoil energy ($E_{\text{available}}$) used in previous analyses of data from MINERvA [13,32,33]. Since the signal requires final state muon plus nucleons only, $E_{\text{available}}$ is the sum of the kinetic energies of all protons, denoted ΣT_p.

Under the assumption of a stationary target neutron in $\nu_\mu + n(\text{bound}) \to \mu^- + p$, energy transfer also can be inferred to be

$$q_0^{(\mathrm{QE})} \equiv \frac{m_p^2 - (m_n - E_b)^2 - m_\mu^2 + 2(E_\mu - p_\mu \cos\theta_\mu)E_\mu}{2(m_n - E_b) - E_\mu + p_\mu \cos\theta_\mu}. \tag{2}$$

Here, m_μ, m_p, and m_n are the masses of the muon, proton, and neutron, E_b is the average binding energy of 34 MeV [6,34,35], and E_μ, p_μ, and θ_μ are the muon energy, momentum, and angle with respect to the neutrino beam. The $q_0^{(\mathrm{QE})}$ of Eq. (2) is the quantity added to the reconstructed muon energy by T2K to estimate neutrino energy of quasielastic-like events, while ΣT_p is the amount added to the muon energy by NOvA to form its neutrino energy estimator for events with quasielastic-like topologies. Combined T2K-NOvA analyses will be credible to the extent that interaction models correctly predict the relationship between these quantities. The measurements of this Letter elicit the correlations among the kinematic variables of quasielastic channels, thereby confronting the models with information of a kind that heretofore has not been available.

The analysis uses high-statistics samples of ν_μ charged-current interactions recorded by the MINERvA detector [36] exposed to the wideband, medium energy NuMI beam [37] at Fermi National Accelerator Laboratory. In the NuMI beam, 120 GeV protons impinging upon a carbon target produce pions and kaons that are subsequently charge-selected, focused by a magnetic horn system, and directed into a pipe where they decay. The resulting neutrino flux is calculated using a GEANT4 simulation of the beam optics with input from hadronic interaction data relevant to the beam and materials [38]. The neutrino flux is constrained by previous measurements of neutrino elastic scattering from atomic electrons, $\nu e^- \to \nu e^-$ [39]. This constraint reduces the normalization uncertainty from 7.8% to 3.9% for muon neutrinos of energies between 2 and 20 GeV. The neutrino interactions occur in the central scintillator tracker of the MINERvA spectrometer, which has a mass fraction of 88.5% carbon, 8.2% hydrogen, 2.5% oxygen, and trace amounts of other elements. Primary vertices of selected events are restricted to a central 5.3 ton region. The spatial resolution of the tracker enables reconstruction of final-state protons and Michel electrons from the $\pi^+ \to \mu^+(\nu_\mu) \to e^+(\nu_e\bar{\nu}_\mu)$ decay chain, as well as the tracks of muons. The magnetized MINOS near detector, located downstream of MINERvA, is used to determine the charge and momenta of exiting muons. The scintillator tracker and the surrounding sampling calorimeters enable calorimetric measurement of ΣT_p and of photon showers from $\pi^0 \to \gamma\gamma$. Occasionally, final-state neutrons leave a small amount of energy that is tagged as a photon or included in ΣT_p; the reference simulation predicts and corrects for this effect. The average ΣT_p for protons is $\approx$250 MeV; neutrons contribute less than 10 MeV of energy in 74% of events and an average of 85 MeV for the rest.

The MINERvA detector response is simulated using GEANT4 [40] version 4.9.4p2 with the QGSP_BERT physics list. The optical and electronics performance is also simulated. Through-going muons are used to determine the absolute energy scale. Full descriptions of calibrations are given in Refs. [36,41]. The absolute energy response to charged hadrons is set according to measurements using a charged particle test beam [42] and a scaled-down version of the MINERvA detector. The effects of accidental activity as a function of beam intensity are simulated by overlaying hits from data in both MINERvA and MINOS.

The reference signal and background models for this analysis are based on a modified version of the GENIE [43] v.2.12.6 event generator. Quasielastic interactions are modeled using the Llewellyn Smith formalism [44] with BBBA05 vector form factors [45] and an axial-vector form factor based on a z-expansion fit to deuterium data [46]. Resonance production is simulated using the Rein-Sehgal model [47] with a dipole axial mass of $M_A^{\mathrm{RES}} = 1.12\ \mathrm{GeV/c^2}$. The nuclear initial state is a relativistic Fermi gas model [48] with $k_F = 0.221\ \mathrm{GeV/c}$ and with a Bodek-Ritchie high momentum tail [49]. Multinucleon quasielastic-like interactions are simulated by the "Valencia model" described in Refs. [10,11,50]. Intranuclear final-state interactions of produced hadrons are modeled using the INTRANUKE-HA package [51].

To better describe MINERvA data, a number of modifications are made in the reference model that are collectively denoted MINERvA tune v4.4.1. The quasielastic cross section is modified as a function of energy and three-momentum transfer based on the random phase approximation of the Valencia model [52,53] appropriate for a Fermi gas [54,55] to account for long-range correlations between nucleons. To account for an observed excess in specific regions of three-momentum transfer and ΣT_p, the multinucleon cross section is increased based on fits to MINERvA data [13] from a lower energy beam configuration. Additionally, based on fits to ν_μ-hydrogen data [56], the nonresonant charged-current pion production is decreased by 43%, the overall baryon-resonance pion production is increased by 15%, and M_A^{RES} is set to 0.94 GeV.

Samples for measuring quasielastic-like interactions and their backgrounds require a muon track that starts in the fiducial volume and is identified in MINOS as negatively charged. All other tracked particles originating from the interaction vertex at the beginning of the muon track must have dE/dx consistent with a proton. Signal and background samples are formed by counting the number of Michel electron candidates within 600 mm long, 600 mm diameter cylinders centered on the neutrino vertex and on endpoints of tracked particles, and by counting isolated clusters constructed from two-dimensional clusters with at least 1 MeV visible energy. The former identify π^+, and the latter identify photons from π^0 decays. Clusters with an

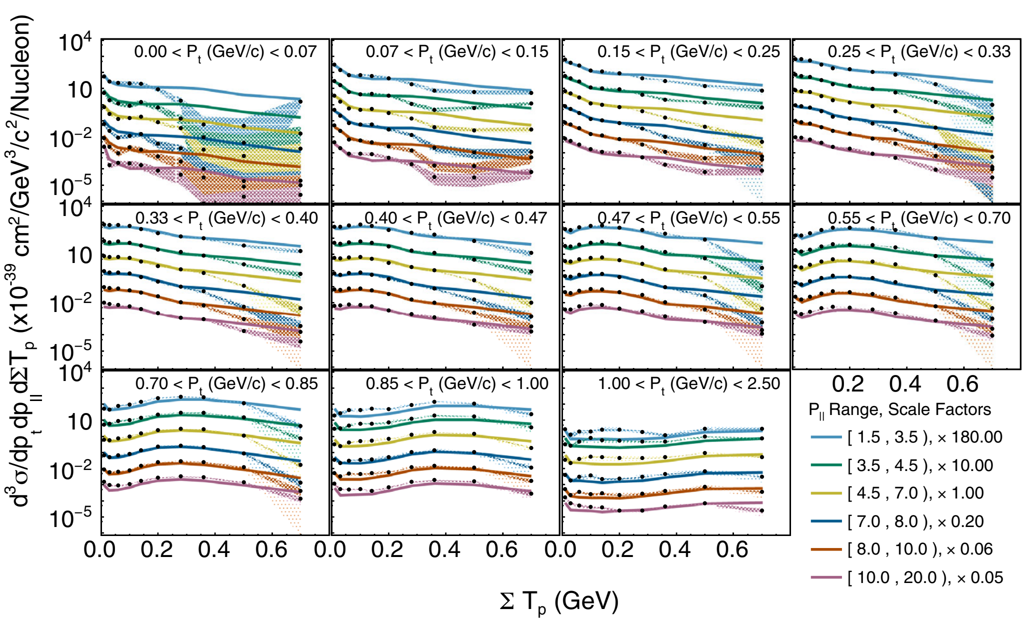

FIG. 1. The flux-averaged triple-differential cross section for quasielastic-like events, $d^3\sigma/dp_{\|}dp_t d\Sigma T_p$, shown as points with colored error bands for designated intervals of $p_{\|}$ in panels of p_t. Note the use of scaling factors and log scale to elicit the trends and consistency across all $p_{\|}$. The predictions of the reference model MINERvA tune v4.4.1 are shown as lines in each panel.

energy less than 10 MeV per hit are assumed to be caused by neutrons producing low energy protons and are not used.

Events that contain either a π^+ (67%), a π^0 (19%), or both (14%), comprise the dominate backgrounds to the quasielastic-like signal. Four exclusive samples are assembled using the criteria of 0 or ≥ 1 Michel electrons, and ≤ 1 or ≥ 2 isolated clusters. Sample A with no Michel electrons and ≤ 1 isolated cluster is the signal sample. Sample B has a Michel electron but ≤ 1 isolated cluster and is rich in single π^+ events. Sample C comprises events with ≥ 2 isolated clusters but no Michel electrons, and is mostly single π^0 events. Sample D events have both Michel electrons and ≥ 2 isolated clusters, and is mostly events with multiple pions. Details of these four samples are given in Ref. [25]. Sample A has 1.3×10^6 selected events with a predicted background of 0.4×10^6. Samples B–D contain 0.23×10^6, 0.22×10^6, and 57 000 events.

For each bin of p_t and ΣT_p, a joint fit to the above-listed four samples is used to determine scale factors applied to the signal sample (A) and to each of the backgrounds [single π^+ (B), single π^0 (C), and multipion (D)]. The fit minimizes a χ^2 over the four scale factors using a singular value decomposition that drops singular values with condition number $< 10^{-3}$ to avoid numerical instability and forbids negative scale factors for any component. The background-subtracted event rate is unfolded using an iterative technique [57] from the RooUnfold framework [58] that is regularized by the number of iterations. A regularization of 10 iterations was chosen by generating randomly fluctuated pseudodata samples with a number of different underlying physics models to ensure fidelity with different assumed data models. The statistical covariance matrix is scaled to account for the finite Monte Carlo statistics in the true-to-reconstructed migration matrix. The unfolded 3D distribution is then corrected for the predicted event loss from selection inefficiencies and detector effects. The average efficiency is between 40% and 75% over all bins. The triple-differential cross section is obtained by normalizing the distribution according to the number of neutrinos incident on the detector and the number of scattering centers. The final result is shown in Fig. 1. To zeroth order, Fig. 1 shows that the reference simulation (solid lines of different colors in the panels) describes the general trends in the data points. Upon closer inspection, discrepancies are apparent. In the lower p_t range of the uppermost panels, for example, the prediction exceeds the data for all $p_{\|}$ for $\Sigma T_p \geq 0.2$ GeV. For clarity, the $p_{\|}$ curves are presented separated in the Supplemental Material [59].

Figure 2 shows the average ΣT_p in each $p_t - p_{\|}$ bin. The average recoil energy in data falls ~50 MeV below the reference model at low p_t, $\lesssim 0.5$ GeV/c, then rises to be comparable to the model ~0.9 GeV/c, and finally exceeds the model prediction in the highest p_t bin. The abrupt change in the highest p_t bins may be due to a cutoff in the Valencia multinucleon model that eliminates this process above three-momentum transfer of 1.2 GeV/c [10,11]. Predictions for GENIE v3.0.6 were produced using NUISANCE [60].

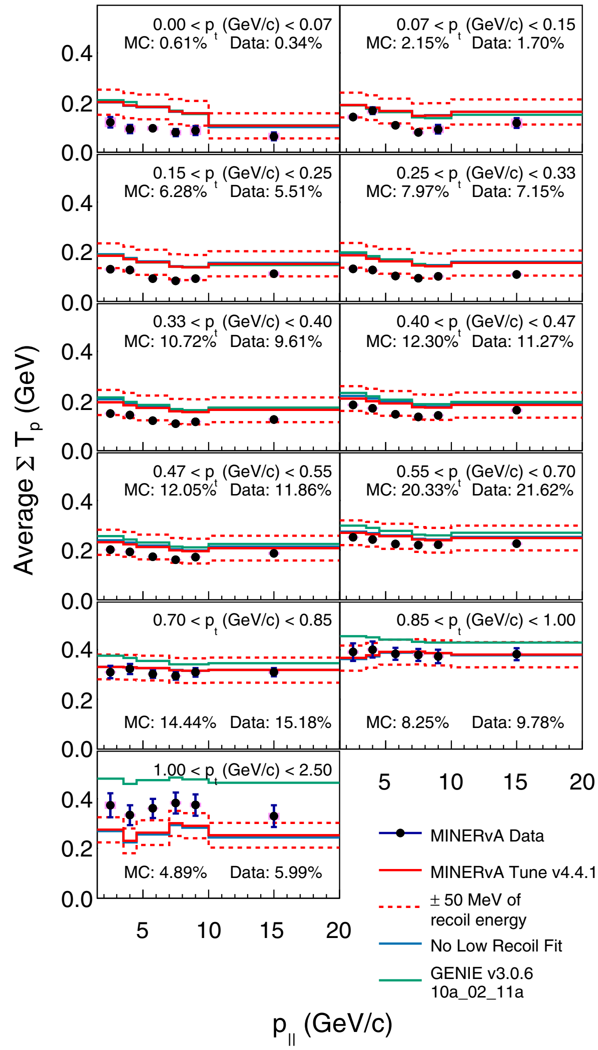

FIG. 2. Distribution of average ΣT_p in $p_t - p_{\|}$ bins. Legends within each panel give the percentage contribution of the p_t panel to the total integrated cross section for data and for the reference simulation. Statistical uncertainty is denoted by the colored box and the total uncertainty by the error bar. The "No Low Recoil Fit" prediction has no enhancement applied to the 2p2h model.

Figures 1 and 2 show discrepancies between data and the reference simulation that persist as a function of $p_{\|}$. Figure 3 displays the ratio of data to simulation at the peak $p_{\|}$ bin, the third from top (yellow) points in Fig. 1. Here the discrepancies can be associated with three different kinematic regions of $p_t - \Sigma T_p$, enumerated below. Since the prominent processes in each region can be identified, each discrepancy suggests specific model developments.

Low p_t, high ΣT_p.—For $0 < p_t < 0.4$ and $\Sigma T_p \geq$ 0.3–0.8 GeV, the reference model predicts significant cross section in a region where the data indicates very little cross section. The predicted events are approximately half

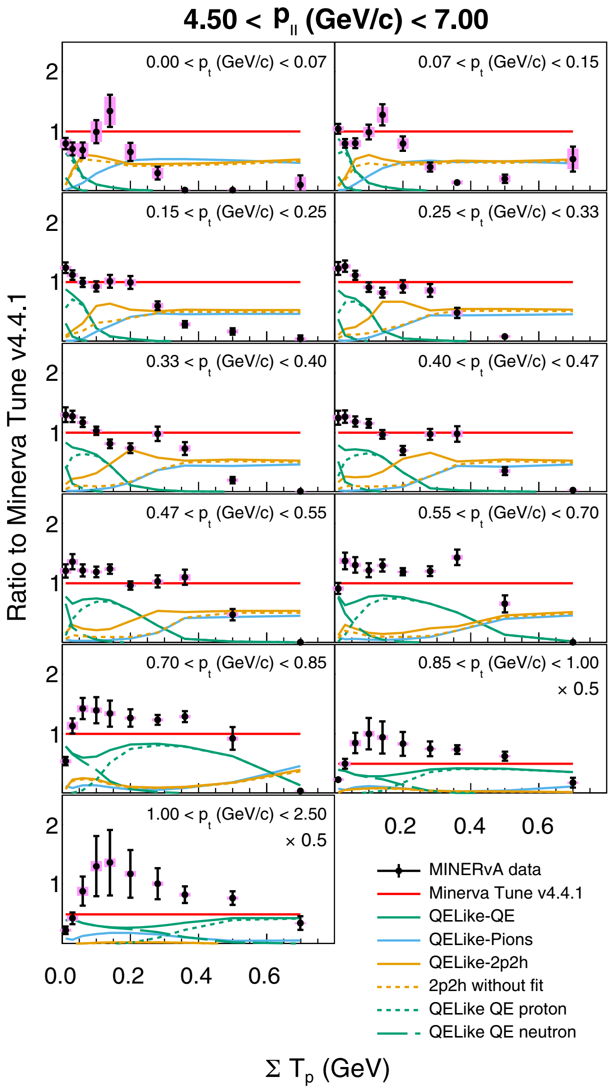

FIG. 3. Ratio of the differential quasielastic-like cross section to predictions in panels of p_t for the peak bin $4.5 < p_{\|} < 7.0$ GeV/c. The predicted cross section in the reference model is broken down into different contributions. Note that in the highest p_t panels, above 0.85 GeV/c, the ratio is shown scaled by 0.5 relative to the other panels. The "2p2h without fit" is the prediction without the 2p2h enhancement. The QE subsample is labeled by the identity of the highest energy nucleon as "QE proton" and "QE neutron." The "QELike-Pions" category includes all events with primary pion production followed by FSI absorption of pions. Additional $p_{\|}$ slices are presented in the Supplemental Material [59].

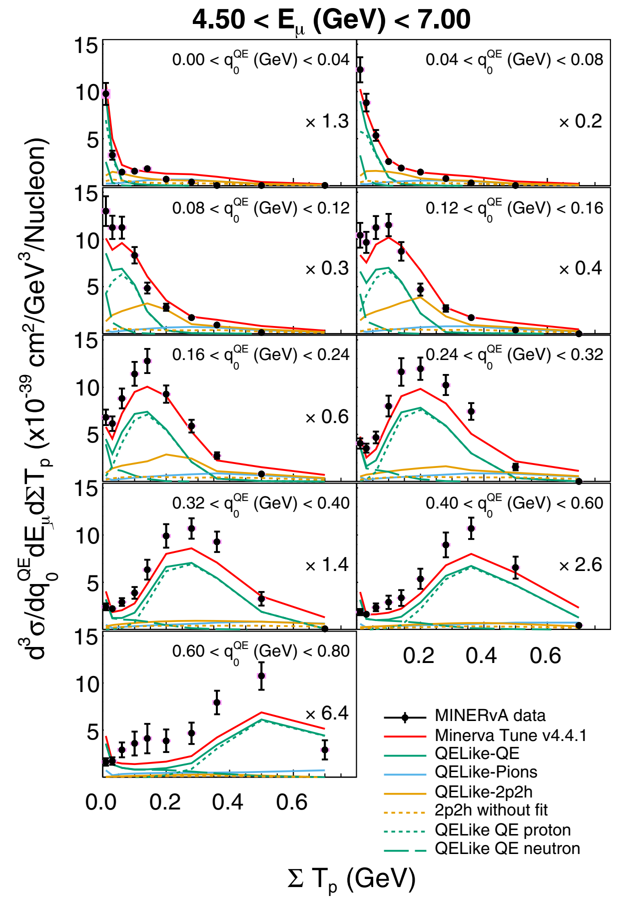

FIG. 4. Flux-averaged triple differential cross section, $d^3\sigma/dE_\mu dq_0^{(\mathrm{QE})} d\Sigma T_p$. Note that scale factors are applied to each of the $q_0^{(\mathrm{QE})}$ panels. Additional $E_{\|}$ slices are presented in the Supplemental Material [59].

multinucleon and half low W pion production where the pion is absorbed in FSI. Therefore, it is likely that both processes are overpredicted. In this region, the multinucleon prediction is from the Valencia model with little effect from MINERvA tune v4.4.1. In pion production, such an effect may arise either from overprediction of the baryon-resonance pion production cross sections or from too-small suppression of primary pions due to FSI. A low Q^2 suppression of resonant pion production[18,61] or a reduction in the visible energy from these events [33], as Fig. 2 also suggests, would improve agreement with this data. Shifts in energy transfers have been observed in (e, e') data for regions of low energy transfer [34,62–70]. An overprediction of pion FSI could arise from finite hadronic formation time [71], an effect not included in the reference simulation. However this background arises mostly from absorption of slow pions ($p_\pi < 0.3$ GeV/c), hence pion formation time is unlikely to account for the entire effect.

Moderate p_t and ΣT_p just above the quasielastic peak.— For ΣT_p of 0.2 GeV and $0.15 < p_t < 0.55$ GeV/c, where the modifications of MINERvA tune v4.4.1 to multinucleon processes are large, the data and reference model would be in strong disagreement without these modifications. Figure 3 shows that the ratio of the data to the reference model dips near the peak of the tune, suggesting that the shape of the MINERvA tune v4.4.1 enhancement may not be accurate, either in rate or in fraction of events with a neutron in the final state. However, at

$p_t > 0.55$ GeV/c, where the model predicts a smaller multinucleon contribution, the data mostly exceeds the reference prediction, suggesting that a significant enhancement to multinucleon processes at higher p_t than in MINERvA tune v4.4.1 may be needed.

High p_t and low ΣT_p.—At $p_t > 0.55$ GeV/c and $\Sigma T_p < 50$ MeV, there is a significant overprediction relative to data. This region is dominated by true quasielastic events where the final-state proton undergoes FSI and leaves the nucleus as one or more energetic neutrons; this suggests that too much strength is given to FSI in this kinematic region.

Figure 4 presents the flux-averaged triple-differential cross section $d^3\sigma/dE_\mu dq_0^{(\mathrm{QE})} d\Sigma T_p$. Here as well, significant data versus reference model discrepancies are seen at low $q_0^{(\mathrm{QE})}$ for ΣT_p beyond the peak of the quasielastic contribution. The previously noted discrepancy at low ΣT_p and high p_t corresponds to a predicted peak near zero ΣT_p at high $q_0^{(\mathrm{QE})}$, which is absent from the data. The cross section in the quasielastic peak is underestimated, especially at higher $q_0^{(\mathrm{QE})}$, and modified form factors could improve this agreement [46,72–74]. This measurement directly probes the relationship between energy estimators used in oscillation experiments, and discrepancies with models suggest deficiencies in modeling those estimators.

In summary, a number of modeling shortfalls for neutrino-nucleus quasielastic-like scattering are identified by this measurement. These imply that relationships between the true neutrino energy of quasielastic-like events and experimental estimators, such as $E_{\mathrm{available}} + E_\mu$ and $q_0^{(\mathrm{QE})} + E_\mu$, differ from those predicted by current neutrino generators. The triple-differential cross section presented in Fig. 4 can serve as a benchmark for neutrino-nucleus interaction simulations employed in ongoing and future neutrino oscillation experiments.

This document was prepared by members of the MINERvA Collaboration using the resources of the Fermi National Accelerator Laboratory (Fermilab), a U.S. Department of Energy, Office of Science, HEP User Facility. Fermilab is managed by Fermi Research Alliance, LLC (FRA), acting under Contract No. DE-AC02-07CH11359. These resources included support for the MINERvA construction project, and support for construction also was granted by the United States National Science Foundation under Grant No. PHY-0619727 and by the University of Rochester. Support for participating scientists was provided by NSF and DOE (USA); by CAPES and CNPq (Brazil); by CoNaCyT (Mexico); by ANID PIA/APOYO AFB180002, CONICYT PIA ACT1413, and Fondecyt 3170845 and 11130133 (Chile); by CONCYTEC (Consejo Nacional de Ciencia, Tecnología e Innovación Tecnológica), DGI-PUCP (Dirección de Gestión de la Investigación—Pontificia Universidad Católica del Peru), and VRI-UNI (Vice-Rectorate for Research of National University of Engineering) (Peru); NCN Opus Grant No. 2016/21/B/ST2/01092 (Poland); by Science and Technology Facilities Council (UK); by EU Horizon 2020 Marie Skłodowska-Curie Action; by an Imperial College London President's PhD Scholarship. D. R. gratefully acknowledges support from a Cottrell Postdoctoral Fellowship, Research Corporation for Scientific Advancement Grant No. 27467 and National Science Foundation Grant No. CHE2039044. We thank the MINOS Collaboration for use of its near detector data. Finally, we thank the staff of Fermilab for support of the beam line, the detector, and computing infrastructure.

[*]Present address: Iowa State University, Ames, Iowa 50011, USA.

[†]Present address: High Energy Physics/Center for Computational Excellence Department, Argonne National Lab, 9700 S. Cass Avenue, Lemont, Illinois 60439, USA.

[‡]Present address: Department of Physics and Astronomy, University of California at Davis, Davis, California 95616, USA.

[§]Present address: Brookhaven National Laboratory, Upton, New York 11973-5000, USA.

[‖]Present address: Los Alamos National Laboratory, Los Alamos, New Mexico 87545, USA.

[¶]Present address: Department of Physics and Astronomy, University of Mississippi, Oxford, Mississippi 38677, USA.

[**]Present address: University of Minnesota, Minneapolis, Minnesota 55455, USA.

[††]Present address: Department of Physics, University of Cincinnati, Cincinnati, Ohio 45221, USA.

[1] K. Abe *et al.* (T2K Collaboration), Phys. Rev. D **91**, 072010 (2015).

[2] P. Adamson *et al.* (NOvA Collaboration), Phys. Rev. Lett. **116**, 151806 (2016).

[3] R. Acciarri *et al.* (DUNE Collaboration), arXiv:1512.06148.

[4] K. Abe, T. Abe, H. Aihara, Y. Fukuda, Y. Hayato *et al.*, arXiv:1109.3262.

[5] A. De Gouvêa, K. J. Kelly, G. V. Stenico, and P. Pasquini, Phys. Rev. D **100**, 016004 (2019).

[6] E. J. Moniz, I. Sick, R. R. Whitney, J. R. Ficenec, R. D. Kephart, and W. P. Trower, Phys. Rev. Lett. **26**, 445 (1971).

[7] O. Benhar, A. Fabrocini, S. Fantoni, and I. Sick, Nucl. Phys. **A579**, 493 (1994).

[8] J. Marteau, Eur. Phys. J. A **5**, 183 (1999).

[9] M. Martini, M. Ericson, G. Chanfray, and J. Marteau, Phys. Rev. C **81**, 045502 (2010).

[10] J. Nieves, I. Ruiz Simo, and M. J. Vicente Vacas, Phys. Rev. C **83**, 045501 (2011).

[11] R. Gran, J. Nieves, F. Sanchez, and M. J. Vicente Vacas, Phys. Rev. D **88**, 113007 (2013).

[12] G. Fiorentini, D. Schmitz, P. Rodrigues *et al.* (MINERvA Collaboration), Phys. Rev. Lett. **111**, 022502 (2013).

[13] P. A. Rodrigues *et al.* (MINERvA Collaboration), Phys. Rev. Lett. **116**, 071802 (2016).

[14] R. Gran *et al.* (K2K Collaboration), Phys. Rev. D **74**, 052002 (2006).

[15] A. A. Aguilar-Arevalo *et al.* (MiniBooNE Collaboration), Phys. Rev. D **81**, 092005 (2010).
[16] G. A. Fiorentini *et al.* (MINERvA Collaboration), Phys. Rev. Lett. **111**, 022502 (2013).
[17] T. Walton *et al.* (MINERvA Collaboration), Phys. Rev. D **91**, 071301 (2015).
[18] P. Adamson *et al.* (MINOS Collaboration), Phys. Rev. D **91**, 012005 (2015).
[19] K. Abe *et al.* (T2K Collaboration), Phys. Rev. D **92**, 112003 (2015).
[20] K. Abe *et al.* (T2K Collaboration), Phys. Rev. D **91**, 112002 (2015).
[21] K. Abe *et al.* (T2K Collaboration), Phys. Rev. D **93**, 112012 (2016).
[22] K. Abe *et al.* (T2K Collaboration), Phys. Rev. D **97**, 012001 (2018).
[23] M. Betancourt *et al.* (MINERvA Collaboration), Phys. Rev. Lett. **119**, 082001 (2017).
[24] X. G. Lu *et al.* (MINERvA Collaboration), Phys. Rev. Lett. **121**, 022504 (2018).
[25] D. Ruterbories *et al.* (MINERvA Collaboration), Phys. Rev. D **99**, 012004 (2019).
[26] K. Abe *et al.* (T2K Collaboration), Phys. Rev. D **98**, 032003 (2018).
[27] T. Cai *et al.* (MINERvA Collaboration), Phys. Rev. D **101**, 092001 (2020).
[28] M. F. Carneiro *et al.* (MINERvA Collaboration), Phys. Rev. Lett. **124**, 121801 (2020).
[29] K. Abe *et al.* (T2K Collaboration), Phys. Rev. D **101**, 112004 (2020).
[30] P. Abratenko *et al.* (MicroBooNE Collaboration), Phys. Rev. D **102**, 112013 (2020).
[31] P. Abratenko *et al.* (MicroBooNE Collaboration), Phys. Rev. Lett. **125**, 201803 (2020).
[32] R. Gran *et al.* (MINERvA Collaboration), Phys. Rev. Lett. **120**, 221805 (2018).
[33] M. V. Ascencio *et al.* (MINERvA Collaboration), arXiv: 2110.13372.
[34] A. Bodek and T. Cai, Eur. Phys. J. C **79**, 293 (2019).
[35] T. Katori, A measurement of the muon neutrino charged current quasielastic interaction and a test of Lorentz violation with the MiniBooNE experiment, Ph.D. thesis, Indiana University, 2008.
[36] L. Aliaga *et al.* (MINERvA Collaboration), Nucl. Instrum. Methods Phys. Res., Sect. A **743**, 130 (2014).
[37] P. Adamson *et al.*, Nucl. Instrum. Methods Phys. Res., Sect. A **806**, 279 (2016).
[38] L. Aliaga *et al.* (MINERvA Collaboration), Phys. Rev. D **94**, 092005 (2016); **95**, 039903(A) (2017).
[39] E. Valencia *et al.* (MINERvA Collaboration), Phys. Rev. D **100**, 092001 (2019).
[40] S. Agostinelli *et al.* (GEANT4 Collaboration), Nucl. Instrum. Methods Phys. Res., Sect. A **506**, 250 (2003).
[41] A. Bashyal *et al.* (MINERvA Collaboration), J. Instrum. **16**, P08068 (2021).
[42] L. Aliaga *et al.* (MINERvA Collaboration), Nucl. Instrum. Methods Phys. Res., Sect. A **789**, 28 (2015).
[43] C. Andreopoulos *et al.*, Nucl. Instrum. Methods Phys. Res., Sect. A **614**, 87 (2010).
[44] C. H. Llewellyn Smith, Phys. Rep. **3**, 261 (1972).
[45] R. Bradford, A. Bodek, H. S. Budd, and J. Arrington, Nucl. Phys. B, Proc. Suppl. **159**, 127 (2006).
[46] A. S. Meyer, M. Betancourt, R. Gran, and R. J. Hill, Phys. Rev. D **93**, 113015 (2016).
[47] D. Rein and L. M. Sehgal, Ann. Phys. (N.Y.) **133**, 79 (1981).
[48] R. A. Smith and E. J. Moniz, Nucl. Phys. **B43**, 605 (1972).
[49] A. Bodek and J. L. Ritchie, Phys. Rev. D **24**, 1400 (1981).
[50] J. Schwehr, D. Cherdack, and R. Gran, arXiv:1601.02038.
[51] S. Dytman, AIP Conf. Proc. **896**, 178 (2007).
[52] J. Nieves, J. E. Amaro, and M. Valverde, Phys. Rev. C **70**, 055503 (2004).
[53] R. Gran, arXiv:1705.02932.
[54] M. Martini, N. Jachowicz, M. Ericson, V. Pandey, T. Van Cuyck, and N. Van Dessel, Phys. Rev. C **94**, 015501 (2016).
[55] J. Nieves and J. E. Sobczyk, Ann. Phys. (Amsterdam) **383**, 455 (2017).
[56] P. Rodrigues, C. Wilkinson, and K. McFarland, Eur. Phys. J. C **76**, 474 (2016).
[57] G. D'Agostini, Nucl. Instrum. Methods Phys. Res., Sect. A **362**, 487 (1995).
[58] T. Adye, *Proceedings of the PHYSTAT 2011 Workshop on Statistical Issues Related to Discovery Claims in Search Experiments and Unfolding* (2011), pp. 313–318, 10.5170/CERN-2011-006.313.
[59] See Supplemental Material at http://link.aps.org/supplemental/10.1103/PhysRevLett.129.021803 provides a separation of $p_{||}$ curves shown in Fig. 1 for a clear presentation of the uncertainty of the measurement and all $p_{||}(E_\mu)$ slices for Figs. 3 and 4 for a complete representation of the triple differential cross sections.
[60] P. Stowell *et al.*, J. Instrum. **12**, P01016 (2017).
[61] P. Stowell *et al.* (MINERvA Collaboration), Phys. Rev. D **100**, 072005 (2019).
[62] A. Bodek and T. Cai, Eur. Phys. J. C **80**, 655 (2020).
[63] A. M. Ankowski, O. Benhar, and M. Sakuda, Phys. Rev. D **91**, 033005 (2015).
[64] S. Boffi, C. Giusti, and F. D. Pacati, Phys. Rep. **226**, 1 (1993).
[65] E. D. Cooper, S. Hama, B. C. Clark, and R. L. Mercer, Phys. Rev. C **47**, 297 (1993).
[66] J. S. O'Connell and R. M. Sealock, Phys. Rev. C **42**, 2290 (1990).
[67] R. M. Sealock *et al.*, Phys. Rev. Lett. **62**, 1350 (1989).
[68] Y. Horikawa, F. Lenz, and N. C. Mukhopadhyay, Phys. Rev. C **22**, 1680 (1980).
[69] A. Papadopoulou *et al.* ($e4\nu$ Collaboration), Phys. Rev. D **103**, 113003 (2021).
[70] A. M. Ankowski and A. Friedland, Phys. Rev. D **102**, 053001 (2020).
[71] T. Golan, C. Juszczak, and J. T. Sobczyk, Phys. Rev. C **86**, 015505 (2012).
[72] K. Borah, R. J. Hill, G. Lee, and O. Tomalak, Phys. Rev. D **102**, 074012 (2020).
[73] A. S. Meyer, A. Walker-Loud, and C. Wilkinson, arXiv:2201.01839.
[74] T. Cai, M. Moore *et al.*, Measurements of Nuclear Effects and the $\bar{\nu}_\mu + H \to \mu^+ + n$ Cross Section in MINERvA with Neutron Tagging, Ph.D. thesis, University of Rochester (2021).